

Document downloaded from:

<http://hdl.handle.net/10251/202523>

This paper must be cited as:

Mayo Nogueira, P.; Ródenas Escribá, FDA.; Verdú Martín, GJ.; Villaescusa, J.; Campayo, JM. (2004). Automatic evaluation of the image quality of a mammographic phantom. *Computer Methods and Programs in Biomedicine*. 73(2):115-128.  
[https://doi.org/10.1016/S0169-2607\(03\)00023-3](https://doi.org/10.1016/S0169-2607(03)00023-3)



The final publication is available at

[https://doi.org/10.1016/S0169-2607\(03\)00023-3](https://doi.org/10.1016/S0169-2607(03)00023-3)

Copyright Elsevier

Additional Information

# AUTOMATIC EVALUATION OF THE IMAGE QUALITY OF A MAMMOGRAPHIC PHANTOM

P. Mayo<sup>\*</sup>, F. Rodenas<sup>\*\*</sup>, G. Verdú<sup>\*</sup>, J. I. Villaescusa<sup>\*\*\*</sup>, J. M. Campayo<sup>\*\*\*\*</sup>

<sup>\*</sup> Dpto. Ingeniería Química y Nuclear, Universidad Politécnica de Valencia, pmayo@iqn.upv.es, gverdu@iqn.upv.es

<sup>\*\*</sup> Dpto. Matemática Aplicada, Universidad Politécnica de Valencia, frodenas@mat.upv.es

<sup>\*\*\*</sup> Servicio de Protección Radiológica, Hospital Universitario La Fe (Valencia), villaescusa\_ign@gva.es

<sup>\*\*\*\*</sup> Unidad Técnica de Protección Radiológica de LAINSA (Valencia), juacames@upvnet.upv.es

## Abstract

In this work a method has been developed to analyse the digital image quality of a mammographic phantom by means of automatic process techniques. The techniques used for the digital image treatment are standard techniques as the image thresholding to detect objects, the regional growing for pixels pooling and the morphological operator application to determine the objects shape and size, etc. This study allows the obtention of information about the phantom characteristics, that due to its small size and lowly contrast can be obtained very difficultly by direct observation. The final aim of this work is to obtain one or more parameters to characterize the reference phantom quality image in an objective way. These parameters will serve to compare images obtained at different mammographic centers and also, to study the temporal evolution of the image quality produced by determined mammographic equipment.

Keywords: mammographic phantom, digital image quality, breast microcalcification detection, computer aided diagnosis.

## 1. INTRODUCTION

The analysis of the image quality obtained from a mammographic phantom of reference, is one of the fundamental points in a complete quality control programme of a mammographic equipment [1,2]. This quality control must analyse the functioning of each one of the elements which participates in the chain of the mammographic image processing: X-ray equipment, radiographic films, development conditions, etc. The good functioning result of all the process must be a mammographic image with an appropriate quality to carry out a suitable diagnostic using the minor possible radiation dose. The quality of the images obtained gives a measurement of the procedure quality for its processing.

A phantom has test objects specifically designed to simulate the breast typical pathologies: microcalcifications, fibres and masses, and it has areas for the image calibration: optical density of

maximum reference (corresponding to the glandular tissue), minimum (characteristic of the adipose tissue) and image resolution, measured as pairs of lines per millimetre. The advantages of the phantoms for the image evaluation are multiple, as we know the test objects that constitutes the phantom and its distribution, we know what to search in the image, also we can obtain images in non clinical conditions with superior radiation dose usually without exposing the patient. Finally, it is possible to obtain as much phantom images as necessary to be compared them between themselves, so it allows to study the image quality evolution carried out by a particular mammographic equipment.

Nowadays, the mammographic image quality is determined in Spain by an expert radiographer or by a radiologist evaluating visually a reference phantom image. He classifies the test objects in three categories: visible, partially visible and not visible, determining the image resolution, that is to say, the line pairs number per millimetre which is able to distinguish and, according to these results, he scores the image according to a scale which determines its quality. It is obvious that this method of evaluating the image quality depends on the human factor, so it makes this subjective determination has a certain variability.

In this work we try to carry out a quality objective evaluation of the mammographic image using reference phantoms, thus we process its digital image in an automatic way using digital treatment techniques of image specifically developed for this type of images, avoiding as far as possible the subjectivity in the image evaluation. The digital image analysis provides information about the phantom characteristics which can be hardly obtained by means of direct observation of the image. Information about the test objects as the size, the exact position, the shape, the orientation, the contrast, etc, allow us to characterize the phantom image obtained and to use these values like parameters in order to determine the image quality. The small size of some test objects and a few contrast, make that in these occasions the objects are not visible for the radiographer or radiologist and there are not detected when the digital image is analysed. So, it is important to establish some visibility criterions for the different test objects, which must be such the system which analyses in an automatic way the phantom image would be able to distinguish as independent objects approximately the same objects number that an expert radiographer or radiologist without introducing new “artificial” objects due to the image noise.

The idea to analyse a reference phantom digital image to determine the image quality produced by a mammographic equipment is not new [3-5]. K.W. Brooks et al [3] develop a image quality programme to establish some visibility criterions for the phantom test objects, which are located using a technique based on the fast fourier transform. D. P. Chakraborty [4] applies an automatic analysis to compare the test images with a pattern image to obtain relations between some of the image parameters and the physical conditions in which the images have been obtained. A.D. Castellano Smith et al [5] develop an algorithm to measure different properties of the phantom, the location of the objects in the image is done with binary masks and the image resolution is measured by calculating the number of zero-crossings of the differential for several profiles at the image resolution area.

The massive screening programmes functioning in many developed countries (see for instance, [6]) carry out the acquisition of a high number of mammographies, each one of them is evaluated by a radiologist. This reason together with the digital technologies, as for the image treatment as for the storage of these ones in digital format, has driven the development of techniques to carry out an automatic analysis of these mammographies. These techniques have in common that they work with the digital image and they make fundamentally a second reading after the radiologist evaluates the image, or stands out the details of the image which help the radiologist to make a correct diagnostic. In the literature there are some works dedicated to the mammography analysis once digitized, for detecting microcalcifications. An usual technique to detect the brilliant areas in the image is the application of filters. In the works [7-9] the laplacian of gaussian filter is used, this filter is implemented as a difference of gaussian filters. The morphological filters are usual tools to study the shape of the microcalcifications [8,10,11]. Another new techniques to detect microcalcifications and to analyse the mammographic image textures are based on the wavelet transform [12-16]; sometimes these techniques are used together with neural networks to select the wavelet coefficients containing the image properties. Another technique to enhance the microcalcifications use fractals to model the image [17].

## 2. METHODOLOGY

### 2.1. Phantom and test objects description

There exists various types of reference phantoms, the fundamental differences are the number of test objects and complexity. The phantom referenced in this work is commercialised by the CIRS firm of model 11-A, SP01 reference. The phantom sketch is reflected in Figure 1, showing the number of test objects, shape and distribution.

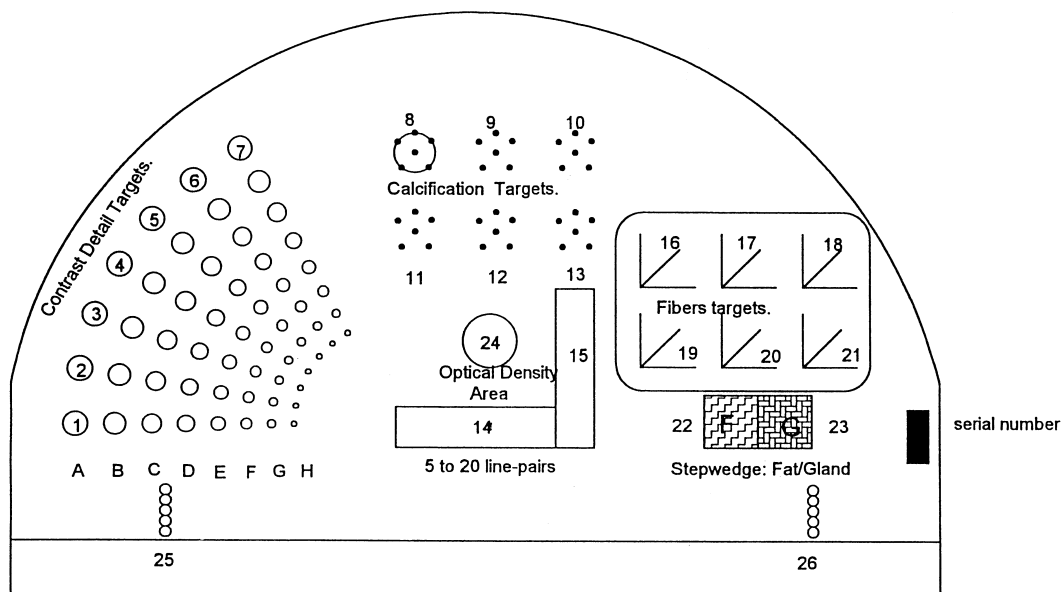


Figure 1: Sketch of the mammographic phantom model 11-A, SP01 reference, CIRS.

The main interest areas in this phantom are the following:

- Contrast detail targets vary in thickness of 4.5 to 0.25 mm (1-7) and in diameter of 4.5 to 1 mm (A-H).
- Microcalcifications targets: group 10 (diameter: 0.300-0.280 mm), group 9 (diameter: 0.250-0.224 mm), group 8 (diameter: 0.212-0.200 mm), group 13 (diameter: 0.160-0.150 mm), group 12 (diameter: 0.140-0.125 mm), group 11 (diameter: 0.112-0.106 mm).
- Horizontal (14) and vertical (15) line pair test targets, from 5 lp/mm to 20 lp/mm .
- Fibers targets: group 16 to 21 (diameter of 1 mm to 0.30 mm).
- Step wedge: adipose tissue (fat: 22) and glandular tissue (gland: 23).
- Radiographical marks:

- Positioning steps (25 and 26): triangles in the low part and circle in the high part.
- Optical density reference area (24).

## 2.2. Film production and digitization

The mammographic equipments which must be controlled do not supply the digital image directly, the mammographic image is formed in a x-ray film which after developing it is fixed in a transparent plate.

Computer image analysis requires the digitization of the phantom radiographic image. Scanning process of the radiographic plate is an important point in this work. The images have been digitized with a slides scanner (AGFA Duoscan f40). It is a charge coupled device (CCD) flatbed scanner. The random noise inherent to all CCD scanners is automatically reduced since each line is scanned several times and the results are averaged.

The resolutions used for film digitization are 600 dpi and 1200 dpi, which produce images of 4265x5673 pixels and 8530x11346 pixels respectively, in grey scale at 8 bits/pixel, that is to say, the grey range is formed by 256 values, which are between black, whose value is 0, and white which corresponds to the value 255.

The response of the scanner is measured by the Modulation Transfer Function (MTF). It specifies the relative amplitude of the output signal as a function of the spatial frequency (lp/mm) of a sinusoidal input signal. The characteristic MTF of the scanner used can be approximated by [18,19]:

$$MTF(f) = \frac{\left| \sin\left(\frac{\pi \cdot f}{dscan}\right) \right|^3}{\left( \frac{\pi \cdot f}{dscan} \right)} \quad \text{if } f \neq 0 \quad (1)$$

where *dscan* is the scanner optical resolution in pix/mm and *f* is the spatial frequency (lp/mm). Using this approximation, the spatial frequency corresponding to 50% and 10% for MTF are 8.6 lp/mm and 14.9 lp/mm at 600 dpi and, 17.3 lp/mm and 29.8 lp/mm at 1200 dpi.

On the other hand, the Nyquist sampling theorem limits the number of line pairs per millimetre that a scanner can resolve. This number is less than half its pixel per millimetre resolution, in our case, less than 12 lp/mm at 600 dpi and 24 lp/mm at 1200 dpi.

### 2.3. Image processing algorithms

Once the image is digitized, it is treated as a matrix  $I$  where the element placed in the file  $i$  and the column  $j$ ,  $I(i,j)$ , represents the pixel located in the file  $i$  and column  $j$  and the value of this matrix element is the grey level of the image in this pixel. The origin of coordinates is fixed in the left superior corner of the image, so that the pixel placed in this corner is  $I(1,1)$ . The object position in the image is indicated giving the pixels coordinates.

Each phantom area requires a specific treatment. The initial image shown in Figure 1 is divided in subimages, so that each one of the phantom interest areas falls into one of the subimages. Each subimage is a matrix of a smaller size than the initial. The coordinates of a determined subimage pixel are related with the coordinates of its pixel in the complete image, adding to the pixel indexes the pixel coordinates of the left superior corner of the subimage. We have considered subimages of each microcalcifications group, of the test objects area which simulate masses, of the area with the lines pairs per millimetre horizontal and vertical, and in the optical density area.

The techniques used for digital image processing are standard techniques [20,21] for the image digital treatment: image thresholding to detect objects, regional growing by pixels attachment, morphological operators application (opening, closing, thinning...), filtered by noise removal, etc.

#### 2.3.1. Microcalcifications location

As it is observed in Figure 1, the microcalcifications area of the phantom is constituted by six groups. The microcalcifications diameter of each one of the groups varies from a group to another, being the group 10 which has the major value and the group 11 the minor. Each group is constituted by six arranged microcalcifications, approximately, in a regular pentagon shape.

As it has been indicated, from each group we form a subimage using the same algorithm in each one of them in order to extract its more important characteristics. For example, in Figure 2 it is showed the blowed up subimage of the group 10 of one of the phantom images.

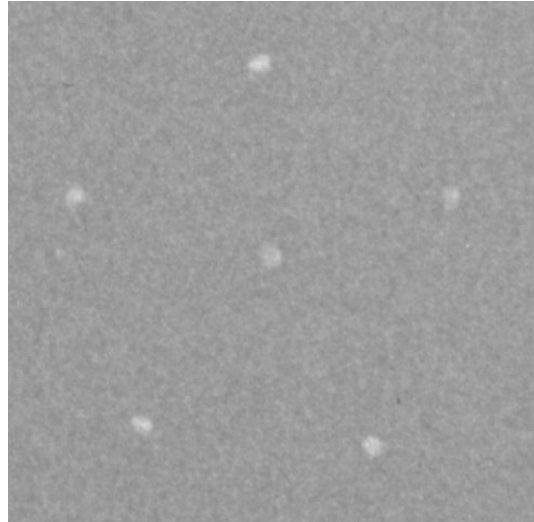


Figure 2: Subimage of the group 10 of microcalcifications of one phantom image.

The first step for the subimage analysis is its segmentation, which consists of detecting and isolating each one of the microcalcifications in the image. The microcalcification identification has been carried out in three stages: thresholding, regional growth and morphological operators application.

#### 2.3.1.1. Thresholding

In this step a threshold to the image has been applied to select the pixels with a grey level larger than the chosen threshold, thus the more brilliant areas of the image are selected. The threshold value selection is a sensible step, as a too high threshold can neglect the microcalcifications which present less contrast, while a too low threshold makes that brilliant points which are selected do not correspond to some microcalcification; these points are caused by the oscillations in the grey levels of the background, due to the noise which contaminates the image. The threshold is chosen by means of pixel area estimation in the subimage corresponding to the microcalcifications group (Figure 2), from the theoretic data of the phantom manufacturing. In order to select the most brilliant pixels of each microcalcification no selecting the brilliant pixels due to the image noise, we have taken as threshold a grey value  $T$  calculated by the formula:

$$(n^{\circ} \text{ of pixels satisfying } I(x,y) > T) = 0.85 \left( \frac{\text{theoretic area of the 6 microcalcifications}}{\text{area of 1 pixel}} \right) \quad (2)$$

This threshold will vary from one group to another, but once its value is calculated for a determined group, it will be the same for all the images of a same reference phantom analysed.

With the thresholding application various areas in the image are chosen which are the first approximation to the microcalcifications, although its shape and size do not coincide with the right one due to the threshold value dependence.

### 2.3.1.2. Regional growing

The second part of the method seeks to improve the first approximation. From each selected area the most brilliant pixel is chosen, the seed pixel, its grey level is represented by  $\underline{E}$ , and from it we apply a standard technique of regional growth to determine the image pixels which belong to a determined microcalcification. This technique consists of three steps:

1. taking a little subimage around the seed with a sufficient size in order to allow the microcalcification to fit and to have a little portion of the background, particularly we take a matrix which size is approximately 16 times the theoretic area of a group microcalcification;
2. estimating in this subimage the average value  $\underline{F}$  and the standard deviation  $\sigma$  of the grey levels of the background and calculating the following value:

$$T = F + 2.5 \sigma \quad (3)$$

this value  $\underline{T}$  must be less than the grey level seed pixel,  $\underline{T} < \underline{E}$ . In other case, we do not consider the possible microcalcification because of it is confused with the image noise;

3. carrying out a sweeping on the subimage pixels selecting those which grey level is larger than  $\underline{T}$  and which are connected to the seed pixel. We mark these pixels as pertaining to the microcalcification.

The result is a binary image of the microcalcifications group in which the value zero is assigned to the background and the value one is assigned to the pixels that belong to the microcalcifications. Graphically, the procedure we have just described consists of selecting as pertaining to the microcalcification the pixels which grey level is 2.5 times the standard deviation over the background average. The justification of this factor is the following: if we suppose that the noise is gaussian, the probability function for a gaussian distribution indicates that the probability

that a pixel corresponding to the background has a grey value which is different in more of  $2.5\sigma$  of the average is 1.24%.

Figure 3 shows the grey level representation around a seed point. In this figure it is observed the peak, which one corresponds to the microcalcification, and the oscillations due to the image noise. Figure 4 shows the full width half maximum (Fwhm) of one of the microcalcifications.

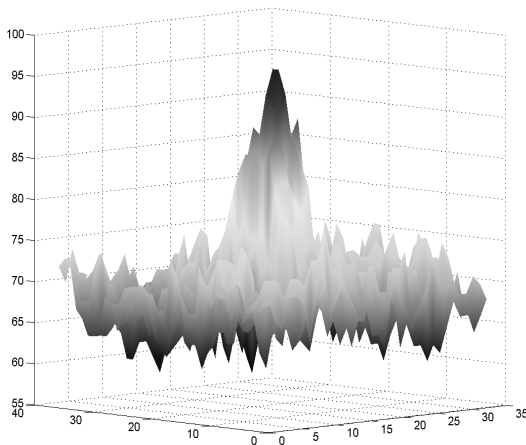


Figure 3: Representation of the grey levels around the seed pixel.

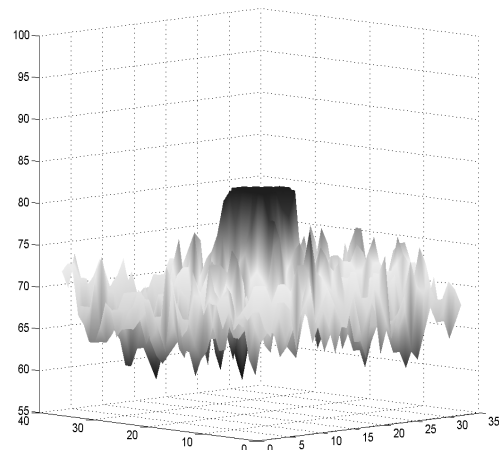


Figure 4: Representation of Fwhm of one of the microcalcifications.

### 2.3.1.3. Morphological operators

Once the possible microcalcifications of a group are detected and the pixels are marked in the initial subimage, a last improving is done. With the threshold it is probable we have selected some pixels or little groups of pixels originated by the noise, or with the regional growth technique it is probable that the microcalcifications present a devilled aspect or has little holes. These defects can be corrected with the application to the image of the opening and closing morphological operators. The use of these and other morphological operators is an usual technique in the image digital treatment [20,21]. The opening and the closing are based on more basic morphological operations denominated erosion and dilation.

The morphological operators take a binary image as input and they turn back a binary image as output. The value of each pixel in the final image depends on the pixel value corresponding to the original image and the pixels value that are around, defining a neighbourhood. The neighbourhood selection with a suitable shape, allows to define sensible morphological operations to determine specific shapes of the objects in the initial image.

The erosion and the dilation operators are the basic transformations in mathematical morphology and constitute the base for more complex morphological operators. Each operation of erosion and dilation uses a determined neighbourhood. The neighbourhood is represented by a “structure element” which is a matrix whose elements are zeros and ones. A structure element can have any size although the more usual dimensions, and that we use in this work, are 3x3. In Figure 5 is represented this structure element:

$S_{11}$	$S_{12}$	$S_{13}$
$S_{21}$	$S_{22}$	$S_{23}$
$S_{31}$	$S_{32}$	$S_{33}$

Figure 5: Structure element of dimensions 3x3, central pixel  $S_{22}$ .

To determine the action of the erosion and the dilation about an input binary image  $\underline{B}$ , a pixel is fixed in the image  $\underline{B}$ , denominated pixel of interest,  $\underline{B}(x,y)$ . On this pixel a structure element is superposed making to coincide the central pixel on the pixel of interest, as is showed in Figure 6:

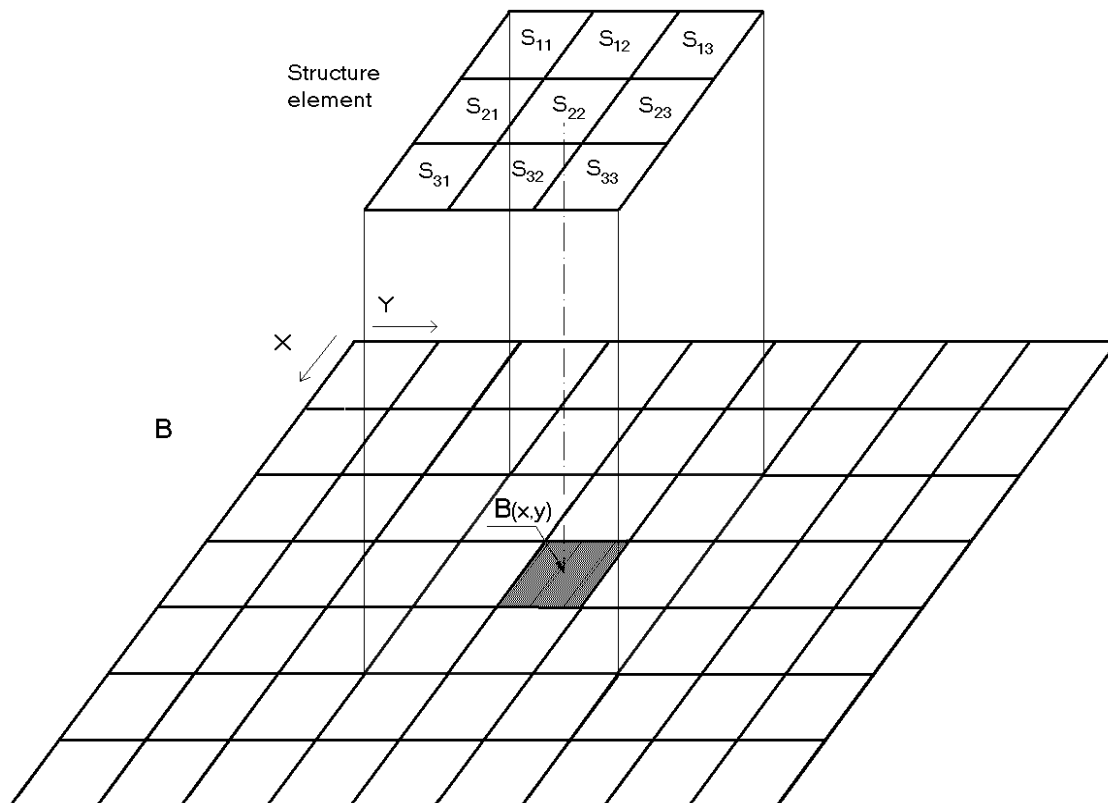


Figure 6: Structure element over the input binary image  $\underline{B}$ .

The central pixel of the structure element represents the pixel of interest, while the other elements with value 1 represent the neighbourhood. The value of the pixel of interest in the output image,  $B_{output}(x,y)$  is calculated using the following rule:

- For erosion, if every pixel in the neighbourhood of the pixel of interest takes the value 1, then the output pixel takes the value 1, in other case it takes the value 0:

$$B(x, y) \rightarrow B_{output}(x, y) = \begin{cases} 1 & \text{if } B(x+i-2, y+j-2) \cdot S_{ij} = S_{ij} \text{ for all } i, j = 1, 2, 3 \\ 0 & \text{in other case.} \end{cases} \quad (4)$$

- For the dilation, if any pixel in the neighbourhood of the pixel of interest takes the value 1, then the output pixel takes the value 1, in other case it takes the value 0:

$$B(x, y) \rightarrow B_{output}(x, y) = \begin{cases} 0 & \text{if } B(x+i-2, y+j-2) \cdot S_{ij} = 0 \text{ for all } i, j = 1, 2, 3 \\ 1 & \text{in other case.} \end{cases} \quad (5)$$

The structure element which has been used in this work is:

1	1	1
1	1	1
1	1	1

Figure 7: Structure element used.

Then, the algorithms to calculate the output image are:

- Erosion:

$$B_{output}(x, y) = \begin{cases} 1 & \text{if } B(x+i-2, y+j-2) = 1 \text{ for all } i, j = 1, 2, 3 \\ 0 & \text{in other case.} \end{cases} \quad (6)$$

- Dilation:

$$B_{output}(x, y) = \begin{cases} 0 & \text{if } B(x+i-2, y+j-2) = 0 \text{ for all } i, j = 1, 2, 3 \\ 1 & \text{in other case.} \end{cases} \quad (7)$$

The effect which produces this erosion form in the binary image objects consists of removing from the selected objects the exterior film of pixels, that is to say, those in contact with the background. The erosion produces the decreasing of the objects size, including the disappearing

if the object is small or extended, and the structure element does not fit in it. The dilation consists of adjoining to the image objects an extra pixels film. The dilation increases the objects size, it closes object holes if there are sufficiently small or decreases its size and it can join two near objects, initially separated.

The morphological operators of opening and closing are based on the concatenated application of the erosion and dilation operators. The opening is defined as an erosion followed by a dilation, and the closing is the dual operation of the opening, then it is based on the dilation application followed by an erosion. The advantages of these operators is that they maintain approximately constant the size objects and furthermore, the opening removes small isolated structures, jetting-out of the object and separates the joined objects by isthmus, while the closing removes small holes and recesses, joining these separated objects. An important property of the opening and the closing is the idempotence which means that the result to apply two consecutive times an opening or closing is the same as to apply them only one time.

We are going to consider the microcalcifications group binary image obtained after applying the regional growth technique to each one of the seed pixels. The selection of the pixels which correspond to each microcalcification in the group subimage, is completed applying an opening to the binary image to remove the isolated points, caused by the noise and rounded off the microcalcifications jetting-out without modifying sizeably the size of the same one, followed by a closing to fulfil eventual holes in the microcalcifications. In this way, we can isolate the microcalcifications of each group characterizing the image pixels (Figure 2) which belongs to each one of the microcalcifications and those pertaining to the background.

#### 2.3.1.4. Features extraction

The last phase of the process consists of extracting the information carried out by the image. Once the microcalcifications are characterized in the image, a big quantity of data about the detected objects characteristics can be obtained: location, size, eccentricity, bright level in relation to the background etc. Particularly, the information analysed for each microcalcifications group is:

1. Identified microcalcifications number in each group.
2. Size of each detected microcalcification. The area is calculated from the pixels number which constitute the object.

3. Full width half maximum (Fwhm). The Fwhm measures the microcalcification pixels area which grey level is superior to the arithmetic average given by  $(\underline{E}+\underline{F})/2$ , being  $\underline{E}$  the grey value of the seed pixel and  $\underline{F}$  the background average in a microcalcification environment. This value can be considered as an alternative estimation of the object size.
4. Centroid position of each microcalcification. We give the coordinates in pixels in the complete phantom image.
5. The eccentricity of each microcalcification which gives an idea of its shape, circular or extended.
6. Microcalcification contrast respect to the background, that is defined [3]:

$$C = M - F \quad (8)$$

being  $\underline{M}$  the average of the pixel grey values of the microcalcification considered and  $\underline{F}$  the background average in a microcalcification environment.

7. Distances of the exterior microcalcifications to the central one, which determine the group radio provided that its a regular pentagon shape. If a distance is very different to the others the detected point must be off, being considered a false finding.
8. Signal-to-noise ratio (SNR) of each microcalcification is calculated applying the formula [20, 21]:

$$SNR = 10 \log_{10} \left( \frac{\sum_{x,y \in \mu Ca} M^2}{\sum_{x,y \in \mu Ca} (I(x,y) - M)^2} \right) \quad (\text{dB}) \quad (9)$$

where the sum is extended for the pixels of the microcalcification considered and  $\underline{I(x,y)}$  represents the pixel grey value in the image. The SNR gives a quantitative measure of the mammographic image quality, thus it indicates the relation signal-noise in the image. We have preferred the definition of the SNR in dB since it is a standard definition usually used in the field of digital image analysis (see, for instance, [20])

### 2.3.2. Line pairs per millimetre calculation

Other important point in the phantom image quality evaluation consists of determining the image resolution. Thus, we have analysed the phantom area in which it appears a lines series each time nearer between themselves, it is identified in the sketch of Figure 1 as the groups 14, 15.

The considered image has 16 vertical lines groups and 16 horizontal ones formed by five brighter lines and five darker lines each one of them, which spatial distribution is 5 to 20 pairs of lines per millimetre. To determine the image resolution means to determine until which group can be discriminated the five lines. To analyse the image and to develop an algorithm which calculates in an automatic way its resolution, we begin considering two subimages, one formed only by the vertical lines (horizontal resolution subimage) and other with the horizontal ones (vertical resolution subimage).

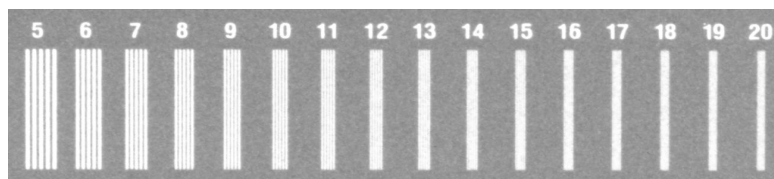


Figure 8: Subimage of horizontal resolution area.

### 2.3.2.1. Thresholding

To number the lines we must isolate them and mark the pixels pertaining to each line. Because of these lines are more brilliant than the background, we begin the segmentation process searching a threshold. In this case the histogram presents two peaks, as it is showed in Figure 9, one of big size corresponding to the background pixels and another smaller corresponding to the lines.

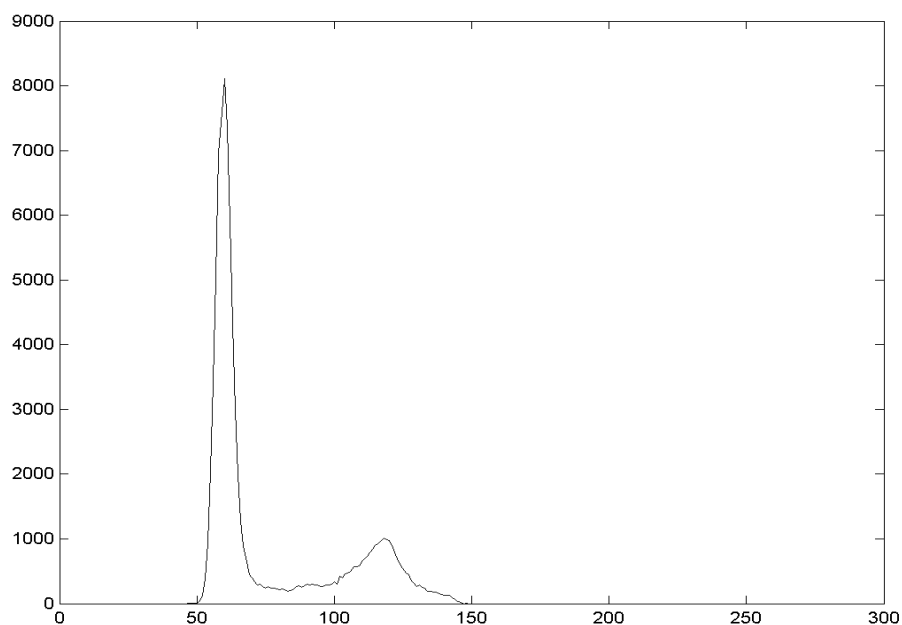


Figure 9: Histogram of the horizontal resolution area.

According to the standard mode of the threshold determination we could take as threshold a grey value near to the minimum between the two peaks, however, this election produces very bad results. The explanation of this fact is that being the lines so near ones to the others, the pixels between lines are more brilliant than the background due to the light diffraction and it must be established another criterion to find the threshold value. The phenomenon can be observed in Figure 10 in which it is showed the grey level representation of a profile in the horizontal resolution area:

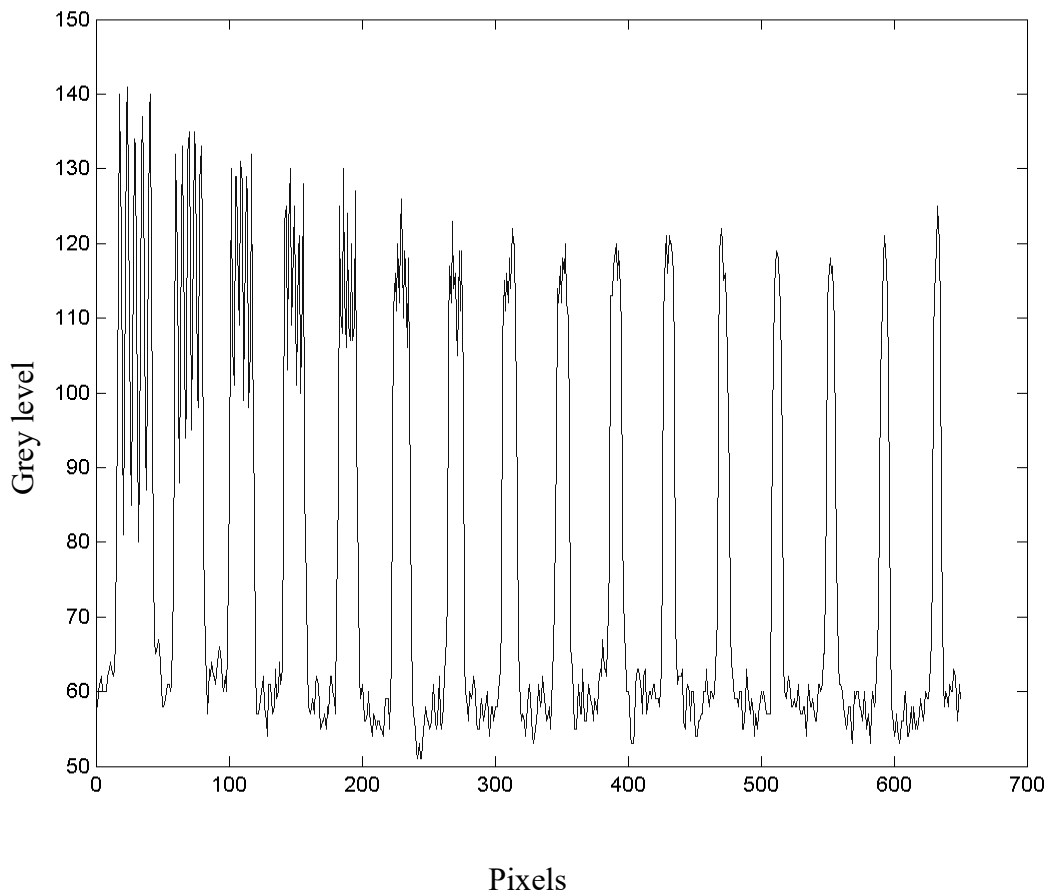


Figure 10: Profile of the horizontal resolution subimage: grey level representation of a row of pixels in the image.

In Figure 10 the maxima correspond to the most brilliant points of the lines (central pixels) and the minima to the pixels between lines. Note how the difference between maxima and minima in each group is reduced while it decreases the distance between the lines (the contrast decreases), however the average value between these maxima and minima is approximately the same for all the groups, this average value is the one we will take as threshold. Furthermore, this threshold value coincides approximately with the grey level corresponding to the maximum of the small peak of the histogram. This observation allows us to calculate in an automatic way the suitable threshold for

each image. For example, the threshold value considered for the image corresponding to Figure 10 is  $T=117$ .

In this figure, when the difference between the maxima and the minima of a group of lines is similar to the noise oscillations, it will be impossible to distinguish the group lines individually. This observation allows a qualitative estimation of the image resolution.

Now, applying the threshold to the subimage given in Figure 8 we obtain a binary image of the horizontal resolution zone. In Figure 11 it is represented the binary image after the threshold.

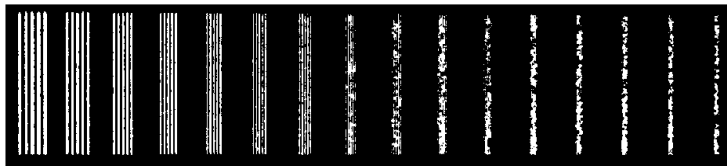


Figure 11: Binary image of the horizontal resolution image.

The threshold process can produce some not desired effects as appearance of small holes in the lines or that two of them are joined in some points, so it makes difficult its visualisation and labelling. To correct these effects we apply to the binary image an opening followed by a closing operators. The effect of these operators on the image have been commented in the previous section.

#### 2.3.2.2. Thinning morphological operator

After thresholding and the morphological operators application to the image, the lines of each group can be clearly identified. So to calculate the image resolution it will be sufficient to count in how many groups are discriminated five independent lines. As our aim is obtaining the resolution in an automatic way, the algorithm must be able to account automatically the lines number of each group, so we reduce the previous lines to lines of one pixel of thickness by means of the application of the morphological operation denominated thinning. This operation has the aim to reduce the object size till converge it in a tracing minimally connected. The idea is similar to the erosion, as the pixels are being removed from the environment object in a successive way taking into account that these pixels cannot be removed as if they would be, the object will be divided in two.

The thinning is carried out with operation type “hit or miss” on the binary image. The process consists of comparing in each input image pixel, the image with a determined structure

element. If they coincide, the pixel of interest value in the output value is zero. In this way the pixel is removed from the object producing the thinning effect. This operation must be repeated for different structure elements. In particular, we have used the following structure elements:

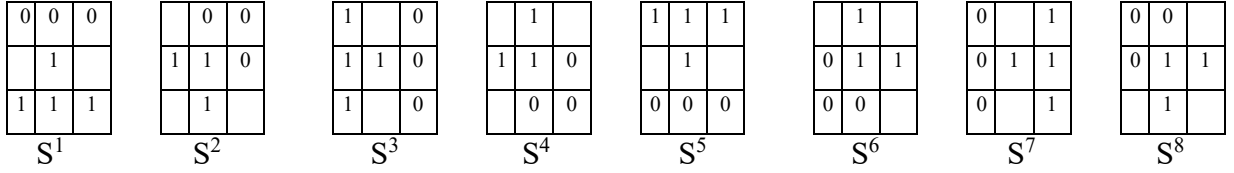


Figure 12: Structure elements used in the thinning. The blank elements represent positions which value “does not mind” in the calculation.

Once processed the image in a successive way with the eight structure elements it begins again with the first one, repeating this process until it does not produce any change in the image. The algorithm can be represented in the following way:

$$B(x, y) \xrightarrow{S^1} B^1(x, y) \xrightarrow{S^2} B^2(x, y) \xrightarrow{S^3} \dots \longrightarrow B_{output}(x, y)$$

$$B^{m+1}(x, y) = \begin{cases} 0 & \text{si } B^m(x+i-2, y+j-2) = S^n ij \text{ for all } i, j \text{ such that } S^n ij \text{ is equal 1 or 0.} \\ B^m(x, y) & \text{in other case.} \end{cases} \quad (10)$$

with  $n = m \bmod(8)$   $y \ m = 0, 1, 2, \dots$  repeating the process until  $B^{m+1} = B^m$ .

After applying the thinning operator to the binary image of Figure 11, the image resolution is calculated counting the lines number per group. We take for it a series of 30 profiles of the binary image obtained after processing it with the thinning operator<sup>1</sup>.

For each profile the algorithm counts the number of ones which it finds and the zeros which exist between them, this allows to decide how many lines exist in each group (see Figure 13). Comparing the obtained results for all the profiles, the lines number in each group is the integer part of the average of the 30 profiles and the resolution is calculated recording the groups where the system has detected five independent lines. It is the same procedure for the horizontal and vertical resolution.

<sup>1</sup>In an alternative way and practically with the same results, it can be used the morphological operation denominated skeletonization which calculates the skeleton or the intern structure of the objects. The difference with the thinning is that the skeletonization uses the distances map, so generally the results vary according to the definition of the considered distance.

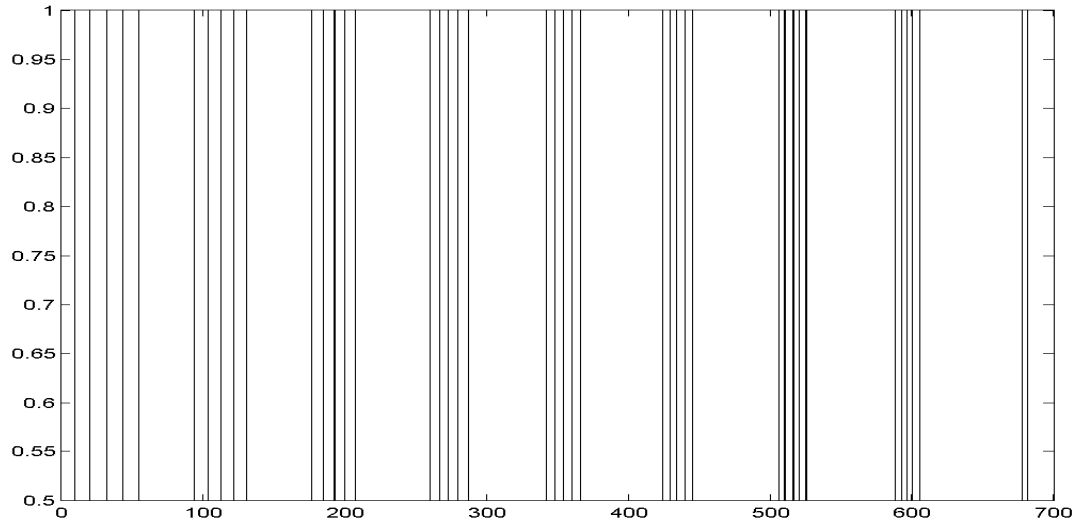


Figure 13: Representation of a profile after thinning of the horizontal resolution image (1200 dpi scanned image).

### 2.3.3. Reference densities areas

Other phantom areas analysed are the corresponding to the reference optical density, 100 % adipose and 100 % glandular tissue density, referenced in the phantom sketch of Figure 1 as 24, 22 and 23 respectively. The reference optical density is the one which has the phantom as background, except in the masses and fibres area. It is composed by 50% of adipose tissue and 50% of glandular tissue. The adipose tissue has less density than the glandular tissue.

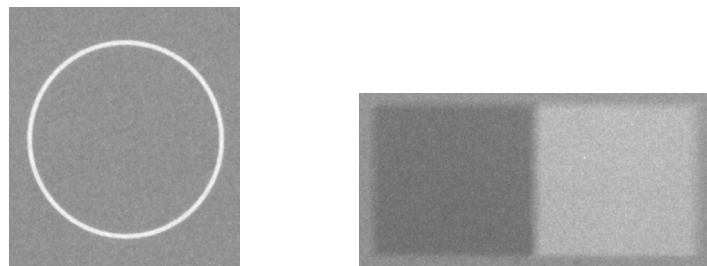


Figure 14: Subimage of the area of the reference optical density, 100 % adipose and 100 % glandular tissue, respectively.

These areas has been characterized by the signal-to-noise ratio value, SNR. To calculate the SNR in each zone of reference, it has taken a subimage containing each zone and the SNR is calculated [20,21]:

$$SNR = 10 \log_{10} \left( \frac{\sum_{x,y \in subimage} M^2}{\sum_{x,y \in subimage} (I(x,y) - M)^2} \right) \quad (\text{dB}) \quad (11)$$

where the sum is extended for the pixels of the subimage considered,  $\underline{M}$  is the average grey level in the subimage and  $\underline{I(x,y)}$  represents the pixel grey value in the subimage.

All the algorithms described above have been implemented in Matlab 6.0 [22].

### 3. RESULTS

The algorithms developed are applied to different images of the phantom, obtained with the same mammographic equipment under different clinical conditions of kV and mAs functioning. Particularly, five images have been considered. Image 1 to 4 are scanned at 600 dpi. Image 1 and 5 are different digitalizations of the same radiographic film. Image 5 is the same as Image 1 but scanned at 1200 dpi. We have chosen this image for comparison purposes.

Tables 1 to 5 show the results for the different microcalcifications groups of each one of the five images. In some of the images all the groups and microcalcifications which are collected in the sketch of Figure 1 of the phantom, have not been detected. This is the reason because there have not been reflected in the tables. In Table 6, the size mean ( $\text{mm}^2$ ) and size variance of each visible group microcalcification of the four images scanned at 600 dpi, are shown.

Table 1: Results of the most significant parameters which characterize the microcalcifications groups of Image 1.

Group visible	N° micro. detected	Size ( $\text{mm}^2$ )	Fwhm ( $\text{mm}^2$ )	Contrast	Distance (mm)	SNR (dB)
10	6	0.124-0.094	0.088-0.070	22.1-15.4	4.142-3.690	26.9-21.3
9	6	0.096-0.060	0.079-0.046	20.6-15.3	4.300-3.216	28.0-23.0
8	6	0.074-0.032	0.050-0.022	20.6-14.1	3.947-3.585	30.1-22.7
13	5	0.076-0.042	0.095-0.047	18.5-13.0	4.146-3.418	31.1-24.6

Table 2: Results of the most significant parameters which characterize the microcalcifications groups of Image 2.

Group visible	N° micro. detected	Size (mm <sup>2</sup> )	Fwhm (mm <sup>2</sup> )	Contrast	Distance (mm)	SNR (dB)
10	6	0.126-0.087	0.097-0.073	21.9-15.0	4.145-3.701	26.2-21.2
9	6	0.093-0.059	0.075-0.043	20.3-15.5	4.308-3.201	27.3-23.2
8	6	0.069-0.034	0.049-0.027	21.1-13.5	3.946-3.593	28.5-22.4
13	5	0.080-0.041	0.083-0.045	18.1-13.2	4.152-3.409	30.1-24.3

Table 3: Results of the most significant parameters which characterize the microcalcifications groups of Image 3.

Group visible	N° micro. detected	Size (mm <sup>2</sup> )	Fwhm (mm <sup>2</sup> )	Contrast	Distance (mm)	SNR (dB)
10	6	0.123-0.064	0.109-0.078	19.0-12.7	4.128-3.677	28.6-23.2
9	6	0.072-0.040	0.078-0.042	18.3-12.1	4.257-3.178	31.3-27.5
8	6	0.062-0.016	0.059-0.030	17.7-12.4	3.911-3.561	31.5-25.5
13	3	0.073-0.055	0.071-0.052	16.0-11.4	3.671-3.352	27.9-25.3

Table 4: Results of the most significant parameters which characterize the microcalcifications groups of Image 4.

Group visible	N° micro. detected	Size (mm <sup>2</sup> )	Fwhm (mm <sup>2</sup> )	Contrast	Distance (mm)	SNR (dB)
10	6	0.159-0.089	0.089-0.055	16.9-11.7	4.102-3.609	23.3-17.4
9	6	0.081-0.058	0.067-0.057	18.6-11.0	4.243-3.215	25.3-22.7
8	6	0.069-0.027	0.061-0.030	15.4-10.9	3.924-3.589	25.8-20.1
13	4	0.086-0.045	0.073-0.046	12.7-8.6	3.747-3.399	26.1-22.0

Table 5: Results of the most significant parameters which characterize the microcalcifications groups of Image 5.

Group visible	N° micro. detected	Size (mm <sup>2</sup> )	Fwhm (mm <sup>2</sup> )	Contrast	Distance (mm)	SNR (dB)
10	6	0.154-0.116	0.081-0.059	33.0-20.9	4.176-3.694	29.3-22.7
9	6	0.101-0.074	0.067-0.040	30.3-20.1	4.324-3.228	29.7-25.0
8	6	0.078-0.043	0.040-0.034	30.7-21.0	3.983-3.627	30.3-23.2
13	4	0.101-0.057	0.054-0.022	25.6-20.7	4.181-3.436	28.8-25.7
12	5	0.020-0.011	0.028-0.014	16.6-14.0	4.100-3.845	38.6-34.0

Table 6: Size mean (mm<sup>2</sup>) and size variance of each visible group microcalcification of the four images scanned at 600 dpi.

Group 10	micro 1	micro 2	micro 3	micro 4	micro 5	micro 6
Size mean	0.112	0.082	0.132	0.977	0.111	0.104
Size variance	3.53E-5	1.81E-4	3.02E-4	7.48E-6	3.12E-5	5.67E-4
Group 9	micro 1	micro 2	micro 3	micro 4	micro 5	micro 6
Size mean	0.075	0.075	0.075	0.055	0.065	0.068
Size variance	2.35E-4	5.71E-4	2.08E-5	1.20E-4	3.50E-4	1.02E-4
Group 8	micro 1	micro 2	micro 3	micro 4	micro 5	micro 6
Size mean	0.048	0.062	0.059	0.063	0.028	0.032
Size variance	1.23E-4	1.23E-4	3.92E-5	1.18E-5	1.22E-4	1.23E-5
Group 13	micro 1	micro 2	micro 3	micro 4	micro 5	micro 6
Size mean	0.048	0.044	0.061	0.073	---	0.059
Size variance	6.49E-5	1.74E-5	9.48E-5	1.84E-4	---	1.32E-4

In Table 7, the horizontal and vertical resolution limits are collected for the five obtained images by means of the automatic method described before. They are compared with the limits which result from the qualitative estimation of the profile resolution represented in Figure 10 (see 2.3.2.2.).

Table 7: Horizontal and vertical resolution limits of the images.

Images	Horizontal (lp/mm)	Vertical (lp/mm)	Qualitative estimation	
			Horizontal (lp/mm)	Vertical (lp/mm)
Image 1	9	8	9	8
Image 2	10	7	10	8
Image 3	9	7	8	7
Image 4	8	7	8	7
Image 5	12	11	9	9

In Table 8 are characterized the reference optical density area, adipose and glandular tissue of the phantom, through the value of the signal-to-noise ratio, SNR.

Table 8: Signal-to-noise ratio of the areas of the reference optical density,  $SNR_{ref}$ , adipose tissue,  $SNR_a$ , and glandular tissue,  $SNR_g$ .

Images	$SNR_{ref}$ (dB)	$SNR_a$ (dB)	$SNR_g$ (dB)
Image 1	26.21	25.65	28.09
Image 2	26.26	25.79	28.14
Image 3	25.83	25.17	27.36
Image 4	25.35	22.23	26.36
Image 5	30.25	30.03	31.56

We have applied statistical tests to the values of Tables 7 and 8, as Pearson and Spearman correlations. The Spearman coefficient between the automatic and qualitative horizontal resolution is 0.73 and between the automatic and qualitative vertical resolution is 0.85. These values near of one indicate that the correlation is positive and stronger for the vertical resolution. The Pearson

coefficient between the  $SNR_{ref}$  and  $SNR_a$  is 0.93, between  $SNR_{ref}$  and  $SNR_g$  is 0.98 and between  $SNR_a$  and  $SNR_g$  is 0.98. These values indicate a very strong correlation.

Also, we can check that the horizontal and vertical resolution of the images obtained following the method, is very consistent with the MTF of the scanner, but although the MTF for the 1200 dpi scanner optical resolution is very high, it is only possible to detect a resolution around 12 lp/mm because the attenuation of the x-ray in the phantom reduces the resolution of the line pair targets.

#### 4. CONCLUSIONS

As we can see from Tables 1 to 6, the calculated size, Fwhm and distance for each microcalcification and each visible group changes slightly in the different images. Moreover, the small variance in the size (see Table 6) confirms that the algorithm works very well identifying clearly the microcalcifications.

Now, if we compare the results for Image 1 and 5, we can assert that better resolution means better contrast, high SNR image and small size microcalcification detected. Thus as we can check, the results for Image 5 show that in this case the small visible group number 12 is detected; the detection of this group by a real observer in normal circumstances using the negatoscope is very difficult.

The results of Table 7 confirm the adequacy of the developed algorithm, improving the qualitative estimation. As we can see, the lines pairs test obtained can be used as a measure of the quality of the image.

The results showed in Table 8 are very consistent, always the SNR of the glandular tissue is higher than the reference and adipose tissues. Furthermore, if we use higher resolution we obtain a better signal-to-noise ratio.

From these results, we see that the developed method can characterize automatically in a suitable way the different phantom areas. The algorithm allows the comparison of different images

between themselves with a master image obtained in determined conditions of mammographic equipment functioning, fixed as reference. Through the comparison we try to know if these images present significant variations in the analysed areas according to the master image, which allows to obtain conclusions with regard to the mammographic equipment functioning for a posterior quality control of this equipment.

The optical resolution of the digital scanner is an influential factor which could affect the most precise results processing, mainly in the calculation of the resolution limit group in the horizontal and vertical resolution area. We consider that a scanner resolution of 1200 dpi is very adequate for the purposes of this work, since typical values for phantom resolution are lower than the limit imposed by Nyquist theorem in this case. More resolution does not imply a substantial improving of the results.

In the near future we will apply this methodology to several controled (kV, mAs, optical density, ...) phantom mammographies to analyse the effect of the controled parameters in the image quality indicators -contrast, SNR, lp/mm and microcalcification size- studied in this work.

## 5. ACKNOWLEDGEMENTS

We are grateful with the European Cancer Screening Programme, EUREF PROJECT 4.3.

## 6. REFERENCES

- [1] Protocolo europeo para el control de calidad de los aspectos físicos y técnicos del cribado mamográfico, European Comission (1996).
- [2] Control de calidad en mamografía, Xunta de Galicia Documentos técnicos de salud pública serie C 2 (1995)
- [3] K.W. Brooks, J.H. Trueblood, K.J. Kearfott and D.T. Lawton, Automated analysis of the American Collegue of Radiology mammographic accreditation phantom images, Medical Physics 24/5 (1997) 709-723.

- [4]. D.P. Chakraborty, Computer analysis of mammography phantom images (CAMPI): An application to the measurement of microcalcification image quality of directly acquired digital images, *Medical Physics* 24/8 (1997) 1269-1277.
- [5] A.D. Castellano Smith, I.A. Castellano Smith and D.R. Dance, Objective assessment of phantom image quality in mammography: a feasibility study, *The British journal of Radiology* 71 (1998) 48-58.
- [6] Programa de Prevención de cáncer de mama en la Comunidad Valenciana, Conselleria de Sanitat Monografies Sanitaries serie E 25 (1998).
- [7] T. Netsch and H.O. Peitgen, Scale-Space Signatures for the Detection of Clustered Microcalcifications in Digital Mammograms, *IEEE Transactions on Medical Imaging* 18/9 (1999) 774-786.
- [8] J. Dengler, S. Behrens and J.F. Desaga, Segmentation of Microcalcifications in Mammograms, *IEEE Transactions on Medical Imaging* 12/ 4 (1993) 634-642.
- [9] G. M. Te Brake and N. Karssemeijer, Single and Multiscale Detection of Masses in Digital Mammograms, *IEEE Transactions on Medical Imaging* 18/7 (1999) 628-639.
- [10] A.J. Méndez, P.G. Tahoces, M.J. Lado, M. Souto and J.J. Vidal, Computer-aided diagnosis: Automated detection of malignant masses in digitized mammograms, *Medical Physics* 25 (1998) 957-964.
- [11] J.M. Mossi and A. Albiol, Digital mammography: Mathematical morphology applied to detection of clusters of microcalcifications, *Proceedings of the IAESTED International Conference on Signal and Image Processing* (1997) 150-153.
- [12] S. Yu and L. Guan, A CAD System for the Automatic Detection of Clustered Microcalcification in Digitized Mammogram Films, *IEEE Transactions on Medical Imaging* 19/2 (2000) 115-126.
- [13] R.N. Strickland, Wavelet Transforms for Detecting Microcalcifications in Mammograms, *IEEE Transactions on Medical Imaging* 15/2 (1996) 218-229.
- [14] T.C. Wang and N.B. Karayiannis, Detection of Microcalcifications in Digital Mammograms Using Wavelets, *IEEE Transactions on Medical Imaging* 17/4 (1996) 498-509.
- [15] L. Costariduo, P Sakellaropoulos, A.P. Stefanoyiannis, E. Ungureanu and G. Panayiotakis, Quantifying image quality at breast periphery vs mammary gland in mammography using wavelet analysis, *The British journal of Radiology* 74 (2001) 913-919.

- [16] A.P. Dhawan, C. Kaiser-Bonasso and M. Moskowitz, Analysis of Mammographic Microcalcifications Using Gray-Level Image Structure Features, IEEE Transactions on Medical Imaging 15/3 (1996) 246-249.
- [17] Huai Li, K.J. Ray Liu and Shih-Chung B. Lo., Fractal Modeling and Segmentation for the Enhancement of Microcalcifications in Digital Mammograms, IEEE Transactions on Medical Imaging 16/6 (1997) 785-798.
- [18] N. Koren. Understanding image sharpness and MTF curves in film, lenses, scanners and sharpening, Website of Norman Koren, [www.normankoren.com](http://www.normankoren.com), 2002.
- [19] R. B. Fagard-Jenkin, R. E. Jacobson, N. R. Axford, A Novel, Approach to the Derivation of Expressions for Geometrical MTF in Sampled Systems", PICS 1999: Image Processing, Image Quality, Image Capture, Systems Conference, 2002.
- [20] R.C. González and R.E. Woods, Digital Image Processing, Addison-Wesley Publishing Company (1993).
- [21] A.K. Jain, Fundamentals of Digital Image Processing, eds. Prentice Hall International (1989).
- [22] Image Processing Toolbox User's Guide for use with Matlab 6.0, Mathworks Inc. (2000)